PHYSICAL REVIEW B VOLUME 52, NUMBER 23 15 DECEMBER 1995-I

Surface morphology of Ge(001) during etching by low-energy ions

S. Jay Chey, Joseph E. Van Nostrand, and David G. Cahill
Department of Materials Science, the Materials Research Laboratory, University of Illinois, Urbana, Illinois 61801
(Received 10 July 1995)

The roughening of a crystalline semiconductor during etching by low-energy ions is characterized using *in situ* scanning tunneling microscopy. Ge(001) surfaces are bombarded by 240-eV Xe ions using a wide range of exposure times and temperatures. Ge dimers are resolved for surfaces etched at $T \geq 165\,^\circ$C and imaged at room temperature. For fixed ion exposure, the roughness increases with increasing temperature; a maximum surface roughness is reached for etching at $\simeq 250\,^\circ$C. At $T \simeq 270\,^\circ$C the character of the surface morphology changes from a relatively disordered arrangement of mounds to a more regular pattern of pits. The isotropy of this pattern formation and the dependence of the in-plane length of the roughness on exposure time suggest that asymmetric kinetics for the attachment of dimer vacancies at ascending versus descending steps drives roughening during etching.

I. INTRODUCTION

A major focus of research on nonequilibrium processes at surfaces is the evolution of surface morphology.[1] Crystal growth at low temperatures is probably the most widely studied nonequilibrium surface process partly due to the importance of interface structure to the synthesis of multilayer thin-film devices. The related problem presented by the etching of crystals by ion sputtering,[2–6] reactive gases,[7,8] or solution chemistry has attracted somewhat less attention despite the critical role etching processes play in the fabrication of microelectronic structures[9] and microanalysis[10,11] techniques. To investigate the intrinsic mechanisms responsible for roughening of a crystal during stochastic removal of atoms from the surface, we study the etching of Ge(001) by low-energy inert gas ions using *in situ* scanning tunneling microscopy (STM).

The close connection between crystal growth and etching in the submonolayer regime is clearly demonstrated by recent studies of ion etching of Si (Ref. 6) and Pt.[12] In the same way that adatoms migrate on surfaces to form islands, surface vacancies migrate and form monolayer deep pits or so-called "vacancy islands." Oscillations in specular reflection high-energy electron diffraction intensities and STM studies show that layer-by-layer etching of Si (Ref. 6) can be achieved under conditions analogous to layer-by-layer epitaxial growth.

Recent studies of multilayer growth and etching demonstrate that these analogies can also be extended to studies of the evolution of surface roughness. On Pt(111), roughening is thought to be driven by asymmetric kinetics for attachment of defects at step edges;[12,13] during growth adatoms incorporate at a higher rate at ascending steps[14] while surface vacancies created by etching have a higher attachment rate at descending steps.[12,13] On a more macroscopic level, these asymmetric kinetics produce a so-called "diffusion bias" for surface defects that destabilizes flat surfaces with respect to the formation of a regular pattern of mounds or pits.[15] Several theoretical investigations[15,16] and experiments on the growth of GaAs(001),[16] Ge(001),[17] and Fe(001) (Ref. 18) by molecular-beam epitaxy (MBE) have stressed the importance of an adatom diffusion bias on the development of surface roughness.

Chason *et al.* also studied the roughening of Ge(001) by Xe-ion bombardment.[5] In Ref. 5, the ion energy was 1 keV ($\sim$ four times larger than our 240-eV Xe ions) and the surface roughness was characterized by x-ray reflectivity, a real-time probe that is complementary to our "quench-and-look" microscopy studies. Roughening kinetics were investigated[5] at 150, 250, 300, and 350 °C. The roughening rate was found to have a maximum at 250 °C. The surface was amorphized by ion bombardment at $T = 150\,^\circ$C and extended ion bombardment at 300 °C produced an anisotropic ripple morphology. These experimental results were modeled in the context of the curvature dependent sputtering rate proposed by Bradley and Harper[19] in combination with surface transport processes that smooth the surface; at high temperatures the surface smoothing process was attributed to the Herring-Mullins mechanism (smoothing rate proportional to a fourth-order derivative of the surface height profile) and at low temperatures the surface smoothing process was attributed to ion-induced viscous relaxation (smoothing rate proportional to a first derivative of the surface height profile).

We do not observe ripple morphologies in our experiments and therefore we have no direct experimental evidence that curvature-dependent sputtering dominates the evolution of surface morphology for our etching parameters, 240-eV Xe and ion current of 1.6 μA cm^2 at an incident angle of 50° from normal. One possible explanation is that the Bradley-Harper mechanism is more isotropic at lower ion energies, suppressing the forma-

0163-1829/95/52(23)/16696(6)/$06.00 ©1995 The American Physical Society

tion of anisotropic ripple morphologies. Alternatively, the Bradley-Harper mechanism for surface roughening may not dominate under our experimental conditions and we must look for another explanation. We believe that our experiments, in combination with previous studies of surface morphology evolution during crystal growth and ion-etching of metals,[12,13] support the assertion that a diffusion bias for surface vacancies can play a dominant role in the roughening of a semiconductor crystal during low-energy ion etching.

II. EXPERIMENTAL DETAILS

Our Ge(001) samples are typically 1.5×1.5 cm^2 and are In bonded to a Mo plate that is subsequently attached to a 3.5-in. diameter Mo sample block using alumina spacers for thermal isolation. After sample introduction, the entire sample block is outgassed at 600 °C for 3 h. The sample is then transferred under ultrahigh vacuum (UHV) to the analysis chamber for ion etching and imaging by STM. During ion etching, the sample is heated by electron-beam bombardment of the Mo backing plate. Temperatures are measured using infrared pyrometry in a wavelength band near 5 μm with a precision of ±10 °C. Cooling rates of the samples are ~ 0.5 °C sec^{-1} at 295 °C and ~ 0.1 °C sec^{-1} at 165 °C.

The Xe-ion beam is produced by a Kaufman-type ion source[21] with a single extraction grid with a 1-mm aperture. After extraction, the ions are electrostatically focused through a 2-mm aperture that separates the differentially pumped chamber housing the ion source from the UHV analysis chamber; the ions are then loosely focused by a second electrostatic lens to an area of 1×1 cm^2. With the ion source hot but with no Xe gas flow, the pressure in the analysis chamber is 5×10^{-10} Torr. The Xe pressure in the analysis chamber is $\sim 1 \times 10^{-8}$ Torr during ion etching.

Ions strike the surface at an angle of 50° from normal with a flux of 1.6 μA cm^2 (1×10^{13} ions cm^2 sec^{-1}) producing a sputtering rate of 0.7 ML min^{-1} determined by analysis of STM micrographs at low ion exposures[12] [see, for example, Fig. 4(a)]. The sputter yield is therefore 0.7 Ge atoms per Xe-ion impact in reasonable agreement with literature values.[22,23] We have studied three exposure times: 15 sec, 10 min, and 3 h corresponding to 0.18, 7, and 130 ML of Ge(001) etched from the surface. The precision of the ion exposures is $\pm15\%$.

To prepare our starting surfaces, we ion etch the Ge crystal for 1 h at 430 °C. The relatively high temperature of this preparation method smooths the roughness of the substrate produced by oxide desorption[20] or prior low-temperature etching and creates a nearly ideal starting surface with large terraces separated by atomic height steps. The average terrace width is $\sim$ 100 nm and reflects the miscut of the Ge crystal, $\sim 0.1°$ in the $\langle 100\rangle$ direction. Smaller area scans of the starting surface reveal a nearly perfect 2×1 dimer reconstruction with a density of atomic scale defects of $< 0.5\%$.

After ion etching, samples are moved to the STM and imaged at room temperature. The data are acquired at a negative sample bias between 1.5 and 2.5 V. At $T \geq 165$ °C, the surface remains crystalline following ion bombardment and we verify the operation of the microscope by checking for well-resolved dimer rows. We therefore are confident that our STM measurements of surface roughness are unaffected by tip-shape artifacts.

III. RESULTS AND DISCUSSION

Images of surface morphologies following ion etching for 3 h are displayed as Fig. 1; this exposure time corresponds to 130 ML of Ge removed from the surface. Smaller area scans (data not shown) reveal small terraces with the 2×1 dimer reconstruction separated by atomic height steps. With increasing temperature, the characteristic in-plane length of the roughness increases, requiring a larger area scan to obtain a complete picture of the morphology. A surprising element of these data is the transition of the morphology from a relatively disordered arrangement of "mounds" to a regular pattern of "pits" at $T \simeq 270$ °C. This multilayer pit formation is reminiscent of experiments on ion etching of Pt(111) (Ref. 12) and suggests that a similar mechanism, asymmetric kinetics for the attachment of surface vacancies at step edges, can drive roughening of a semiconductor surface.

To quantify the roughness, we evaluate the height difference correlation function,[24] $G(\rho) = \langle(h_j - h_i)^2\rangle$, where h_j and h_i are the heights of the surface at two locations labeled by i and j separated by a distance ρ. The brackets signify an average over pairs of points i, j separated by ρ. $G(\rho)$ is related to the height-height correlation function $H(\rho) = \langle h_j h_i\rangle$ by $G(\rho) = 2\langle W^2\rangle - 2H(\rho)$ where $\langle W^2\rangle = \langle(h_i - \langle h_i\rangle)^2\rangle$. Examples of $H(\rho)$ and $[G(\rho)]^{1/2}$ for two of the etched surfaces shown in Fig. 1 are plotted in Fig. 2. Data for a typical starting surface are included in Fig. 2(b) for comparison and reveal background effects due to uncompensated curvature in the STM images.

We focus our attention on two aspects of these correlation functions. First, we define d by the position ρ of a local minimum in $G(\rho)$ [or, equivalently, the position of the first local maximum in $H(\rho)$] that corresponds to the separation or repeat distance between dominant features in the surface morphology, see Fig. 2. The location of d is marked in Fig. 2 by arrows. The size of the first local maximum $H(d)$ is typically only 2–5 % of $H(0)$ but the position of d is in fact easily determined and reproducible. Second, we note that $G(\rho)$ has a local maximum [and $H(\rho)$ a local minimum] near $\rho = d/2$. We therefore use $G(d/2)$ as a measure of the vertical roughness of the film. We prefer this measure of the roughness to the more commonly used large ρ limit of $G(\rho)$ because STM data can be affected by artifacts at large length scales.

The vertical roughness $[G(d/2)]^{1/2}$ of 14 ion-etched surfaces are plotted in Fig. 3 as a function of the temperature of the crystal during etching. We observe that following 130 ML etched from the surface, an increase in temperature within the temperature interval $165 < T <$

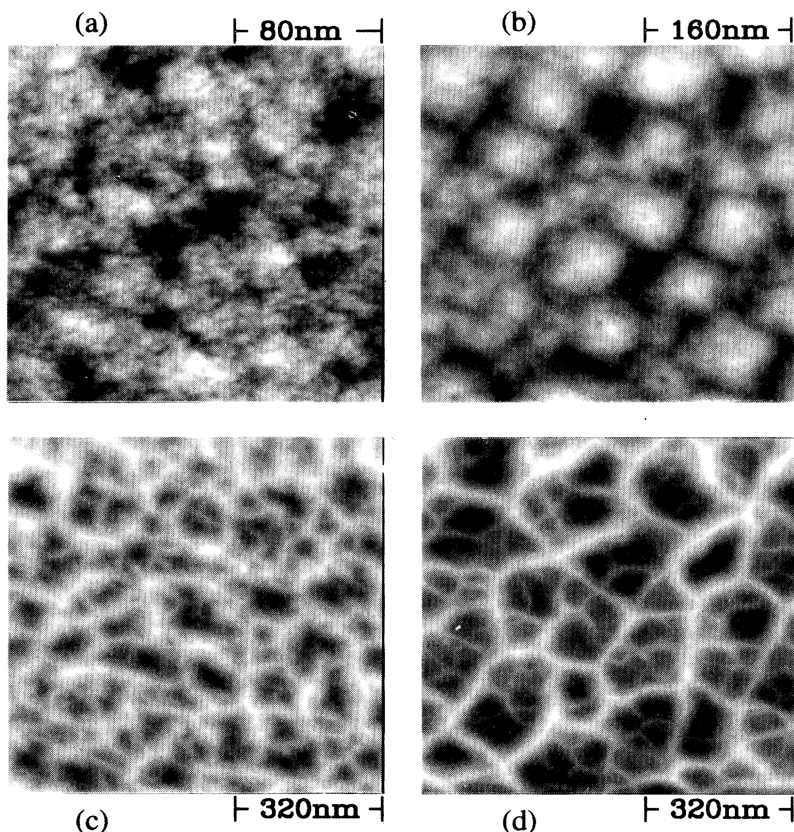

FIG. 1. STM images of Ge(001) etched by 240 Xe ions for 3 h at a flux of 1×10^{13} ions cm^{-2}, corresponding to 130 ML etched from the surface. Scale bars are shown next to each image. Temperature of the Ge(001) crystal during etching, and the black-to-white gray scales are (a) 165 °C, 1.2 nm; (b) 220 °C, 2.9 nm; (c) 270 °C, 3.3 nm; and (d) 295 °C, 3.3 nm. In (a) and (b) the ion etching produces a relatively disordered arrangement of mounds. In (c) and (d), we observe a pattern of pits.

220 °C produces an increase in roughness, in qualitative agreement with the results of Ref. 5. Data for crystals etched to a depth of 7 ML behave similarly. For submonolayer etching, the roughness decreases slightly with temperature; at $T \simeq 165$ °C, many of the adatoms produced during ion impacts do not recombine with neighboring vacancies and adatom islands are formed.[3,6]

Surface roughening is often modeled as a balance between processes that smooth the surface and mechanisms that drive roughening.[1,5] In Ref. 5, the reduced rate of roughening at $T \leq 165$ °C was attributed to viscous relaxation of the amorphized surface. After ion bombardment at 165 °C and cooling to room temperature, we observe by STM that the surface is crystalline. Since we do

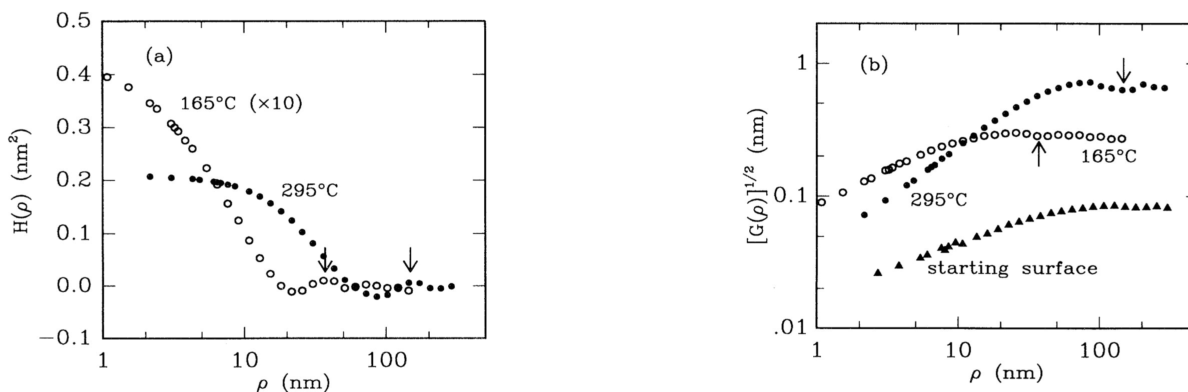

FIG. 2. (a) Height-height correlation function $H(\rho)$ of surface points separated by a distance ρ for the surfaces shown in Figs. 1(a) (130 ML removed at 165 °C) and 1(d) (130 ML removed at 295 °C). Arrows mark the local maximum of $H(\rho)$ that is used to characterize the in-plane length scale of the surface roughness. Data for etching at 165 °C have been multiplied by a factor of 10 for display. (b) Square root of the height difference correlation function $[G(\rho)]^{1/2}$ of the same two surfaces as in part (a). Data for the starting surface are included for comparison.

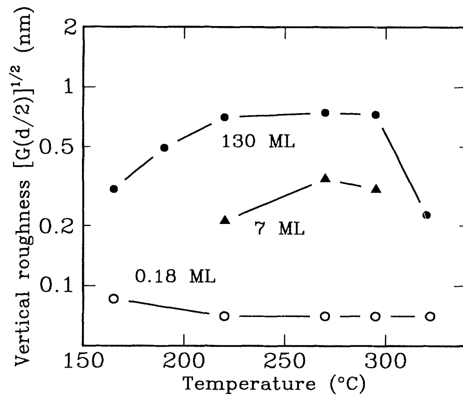

FIG. 3. Vertical surface roughness of Ge(001) etched by 240-eV Xe ions at temperature T. $G(d/2)$ is approximately equal to $2\langle(h_i - \langle h_i\rangle)^2\rangle$. Data for three etching times are shown: solid circles, 130 ML removed; solid triangles, 7 ML; open circles, 0.18 ML.

not have a real-time diffraction probe available to us to evaluate surface structure, we cannot conclusively state that the surface remains crystalline during ion bombardment at 165 °C; the possibility remains that the surface is amorphized during bombardment and then recrystallizes during the time required to cool the sample to room temperature. We have attempted to study this possibility by creating an amorphized surface by ion bombardment at room temperature for 3 h and subsequently annealing the sample at 165 °C for 20 min. We have not been able to image the dimer reconstruction on amorphous surfaces subjected to this annealing schedule and conclude that a fully amorphized surface cannot recrystallize during cooling from 165 °C.

If we make the assumption that the surface remains crystalline during bombardment at $T \geq 165\,°C$, viscous relaxation cannot play a role in this temperature range. The kinetics of smoothing processes on a crystalline surface can only increase with temperature. Therefore, we believe that the mechanism driving surface roughening is strongly temperature dependent.

We propose that this temperature-dependent mechanism for surface roughening is a diffusion bias[15] for vacancies. In other words, we hypothesize that vacancies have faster attachment kinetics at descending steps relative to ascending steps.[12] While the dimer reconstruction of the Ge(001) surface greatly complicates an assignment of atomic-level mechanisms, we envision that a dimer vacancy approaching a descending step sees little or no energetic barrier for reaching the step edge, while a vacancy approaching an ascending step encounters a more significant barrier for moving up to the next terrace. For low-temperature epitaxial growth of Fe(001) (Ref. 18) and Ge(001),[17,25] a diffusion bias for adatoms drives surface roughening and the in-plane length scale of the roughness d evolves continuously from the island spacing during the first monolayer of growth. The dependence of d on film thickness t approximates a power law, $d \propto t^{\gamma}$ with $\gamma = 0.16$ for Fe(001) grown at room temperature[18]

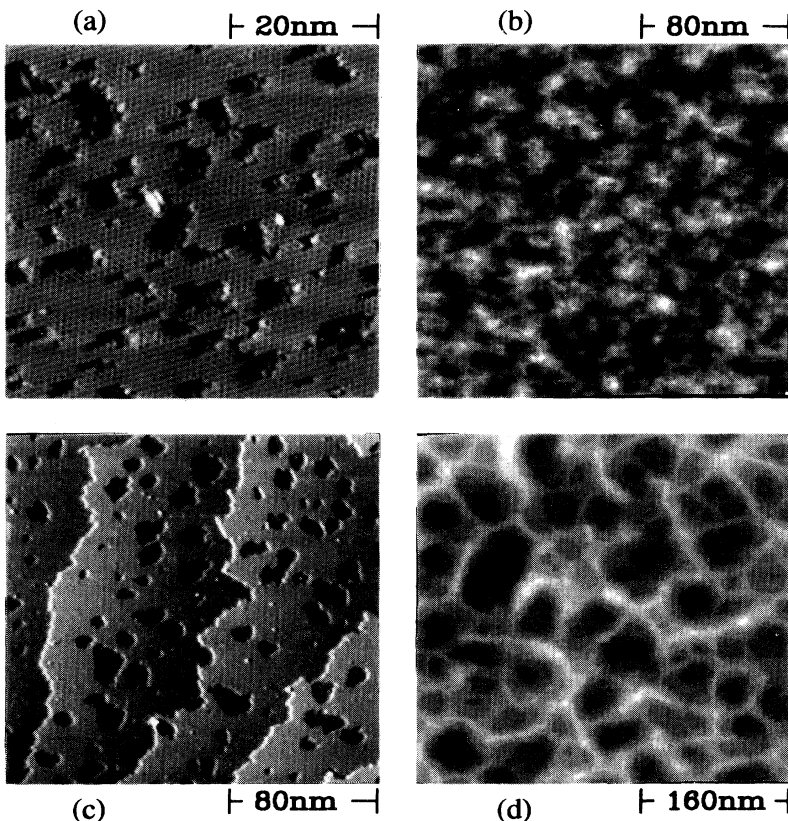

FIG. 4. STM images of Ge(001) etched by 240 Xe ions. Scale bars are shown next to each image. Number of monolayers removed and temperature during etching are: (a) 0.18, 220 °C; (b) 7.0, 220 °C; (c) 0.18, 295 °C; (d) 7.0, 295°C. In (a) and (c) the images have been high pass filtered to increase step edge contrast. In (b) and (d) no filter is used and the black-to-white gray scales are 0.9 nm and 1.3 nm, respectively.

and $\gamma = 0.42$ for Ge(001) grown at 155 °C.[17,25] If a diffusion bias for vacancies plays a dominant role in creating surface roughness during etching, we can expect that d will evolve in a similar manner.

STM images for lower ion exposure times are shown in Fig. 4 and our analysis of the in-plane length scale d is shown in Fig. 5. After 0.18 ML of etching, vacancy islands are observed on the large terraces of the starting surface, see Figs. 4(a) and 4(c). One adatom island is also visible in Fig. 4(a), etching temperature $T = 220$ °C. The average separation between vacancy islands increases rapidly at $T \simeq 300$ °C, see Fig. 5(a), a behavior that we attribute to Ostwald ripening. A fit to the data for $T \leq 225$ °C, gives an effective activation energy of 0.23 ± 0.02 eV for the vacancy island separation. Converting this effective activation energy to an activation energy for dimer vacancy diffusion[26] requires knowledge of the anisotropy of diffusion and attachment kinetics[27] and is outside the scope of this work.

Images of Ge(001) following 7 ML etched from the surface [see Figs. 4(b) and 4(d)] already show the same characteristics as the morphology following more extended etching. For the three etching temperatures plotted in Fig. 5(b), 220, 270, and 295 °C, the in-plane length scale d shows an approximate power-law dependence on etching time and evolves continuously from the vacancy island separation during submonolayer etching.[28] This coarsening behavior supports our picture of an intrinsic roughening mechanism resulting from a diffusion bias for vacancies.

On the Pt(111) surface,[13] an asymmetry in the width of denuded zones adjacent to ascending and descending steps was directly observed, confirming the existence of a diffusion bias for vacancies on this surface. Unfortunately, a similar analysis of vacancy island distributions on Ge(001) has not yielded a significant asymmetry in the widths of denuded zones (data not shown). The asymmetries in step-edge kinetics for vacancies and adatoms on Ge(001) may be too subtle to observe in this direct manner. Despite the fact that the surface morphology of Ge(001) (Ref. 17) shows a striking resemblance to growth models that include step-edge barriers,[16] studies of denuded zone widths during MBE growth of Si(001) (Ref. 29) and Ge(001) (Ref. 25) have failed to reveal asymmetric attachment kinetics for adatoms.

We do not yet understand why the character of the morphology changes from mounds to pits at $T \simeq 250$ °C. Since the roughness decreases rapidly after only a small increase in temperature to $T \simeq 300$ °C, see Fig. 3, the change in character may be connected to the rapidly increasing kinetics of processes responsible for surface smoothing. Adatom emission from step edges may destabilize small adatom islands and favor the formation of pits relative to mounds. Experiments on the kinetics of smoothing with and without ion bombardment and experiments on the microscopic nature of vacancy kinetics on Ge(001) are in progress.

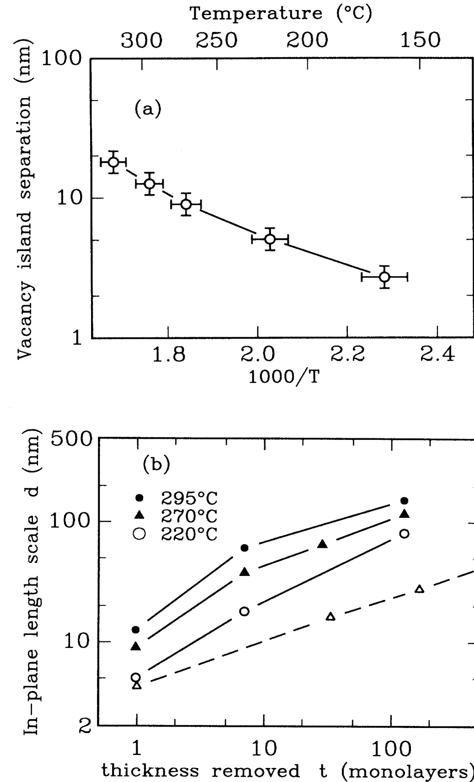

FIG. 5. (a) Average separation between vacancy islands d following 0.18 ML removed and plotted as a function of reciprocal temperature. (b) Characteristic in-plane length scale d of the surface roughness plotted as a function of the thickness removed by ion etching t. Data points for 0.18 ML removed are plotted at $t = 1$ (1 ML) since the vacancy island separation is a weak function of etching time during submonolayer etching, see Ref. 27. Solid lines connect data points for crystals etched at the same temperature: solid circles, 295 °C; solid triangles, 270 °C; open circles, 220 °C. Dashed line is for Ge(001) crystal growth by molecular-beam epitaxy at 155 °C, see Ref. 25.

ACKNOWLEDGMENTS

This work was supported by U.S. Department of Energy Grant No. DEFG02-91-ER45439 through the University of Illinois Materials Research Laboratory and the Donors of the Petroleum Research Fund. We thank P. Bedrossian for helpful discussions and J. Stroscio for sending a copy of his recent work prior to publication.

[1] D. D. Vvedensky, A. Zangwill, C. N. Luse, and M. R. Wilby, Phys. Rev. E **48**, 852 (1993).

[2] G. K. Wehner, J. Appl. Phys. **29**, 217 (1958).

[3] S. T. Picraux, D. K. Brice, K. M. Horn, J. Y. Tsao, and E. Chason, Nucl. Instrum. Methods Phys. Res. Sect. B **48**, 414 (1990).

[4] E. Chason, J. Y. Tsao, K. M. Horn, S. T. Picraux, and H. A. Atwater, J. Vac. Sci. Technol. A **8**, 2507 (1990).

[5] E. Chason, T. M. Mayer, B. K. Kellerman, D. T. McIlroy, and A. J. Howard, Phys. Rev. Lett. **72**, 3040 (1994).
[6] P. Bedrossian, Surf. Sci. **301**, 223 (1994).
[7] D. Rioux, R. J. Pechman, M. Chander, and J. H. Weaver, Phys. Rev. B **50**, 4430 (1994).
[8] J. V. Seiple and J. P. Pelz, Phys. Rev. Lett. **73**, 999 (1994).
[9] Harold F. Winters and J. W. Coburn, Surf. Sci. Rep. **14**, 161 (1992).
[10] Eun-Hee Cirlin, John J. Vajo, and T. C. Hasenberg, J. Vac. Sci. Technol. B **12**, 269 (1994).
[11] K. Elst, W. Vandervorst, J. Alay, J. Snauwaert, and L. Hellemans, J. Vac. Sci. Technol. B **11**, 1968 (1993).
[12] Thomas Michely and George Comsa, Nucl. Instrum. Methods Phys. Res. Sect. B **82**, 207 (1993).
[13] Thomas Michely, Terry Land, Uffe Littmark, and George Comsa, Surf. Sci. **272**, 204 (1992).
[14] Gert Ehrlich and F. G. Hudda, J. Chem. Phys. **44**, 1039 (1966).
[15] J. Villain, J. Phys. (France) I **1**, 19 (1991).
[16] M. D. Johnson, C. Orme, A. W. Hunt, D. Graff, J. Sudijono, L. M. Sander, and B. G. Orr, Phys. Rev. Lett. **72**, 116 (1994).
[17] Joseph E. Van Nostrand, S. Jay Chey, M.-A. Hasan, David G. Cahill, and J. E. Greene, Phys. Rev. Lett. **74**, 1127 (1995).
[18] Joseph A. Stroscio, D. T. Pierce, M. Stiles, A. Zangwill, and L. M. Sander (unpublished).
[19] R. Mark Bradley and James M. E. Harper, J. Vac. Sci. Technol. A **6**, 2390 (1988).
[20] X.-J. Zhang, G. Xue, A. Agarwal, R. Tsu, M.-A. Hasan, J. E. Greene, and A. Rockett, J. Vac. Sci. Technol. A **11**, 2553 (1993).
[21] J. M. E. Harper, J. J. Cuomo, P. A. Leary, G. M. Summa, H. R. Kaufman, and F. J. Bresnock, J. Electrochem. Soc. **128**, 1077 (1981).
[22] D. Rosenberg and G. K. Wehner, J. Appl. Phys. **33**, 1842 (1962).
[23] E. Chason, P. Bedrossian, K. M. Horn, J. Y. Tsao, and S. T. Picraux, Appl. Phys. Lett. **57**, 1793 (1990).
[24] Jean Lapujoulade, Surf. Sci. Rep. **20**, 191 (1994).
[25] Joseph E. Van Nostrand, S. Jay Chey, and David G. Cahill, J. Vac. Sci. Technol. B **13**, 1816 (1995).
[26] Single atom vacancies are thought to decay rapidly into dimer vacancies, see Zhenyu Zheng and Horia Metiu, Phys. Rev. B **48**, 8166 (1993).
[27] Jacques Villain, Alberto Pimpinelli, Leihan Tang, and Dietrich Wolf, J. Phys. (France) I **2**, 2107 (1992).
[28] While the data for d versus t approximate a power law, we do not observe a single, well-defined power law for a large range of t and are therefore unable to apply a quantitative scaling analysis to our data.
[29] Y.-W. Mo and M. G. Lagally, Surf. Sci. **248**, 313 (1991).

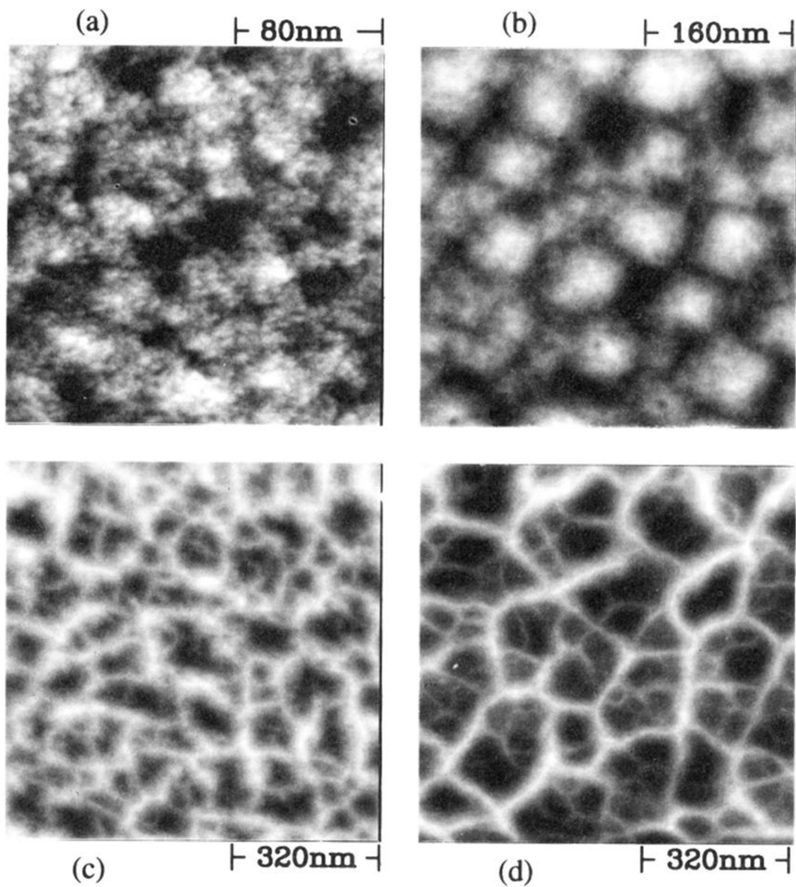

FIG. 1. STM images of Ge(001) etched by 240 Xe ions for 3 h at a flux of 1×10^{13} ions cm^{-2}, corresponding to 130 ML etched from the surface. Scale bars are shown next to each image. Temperature of the Ge(001) crystal during etching, and the black-to-white gray scales are (a) 165 °C, 1.2 nm; (b) 220 °C, 2.9 nm; (c) 270 °C, 3.3 nm; and (d) 295 °C, 3.3 nm. In (a) and (b) the ion etching produces a relatively disordered arrangement of mounds. In (c) and (d), we observe a pattern of pits.

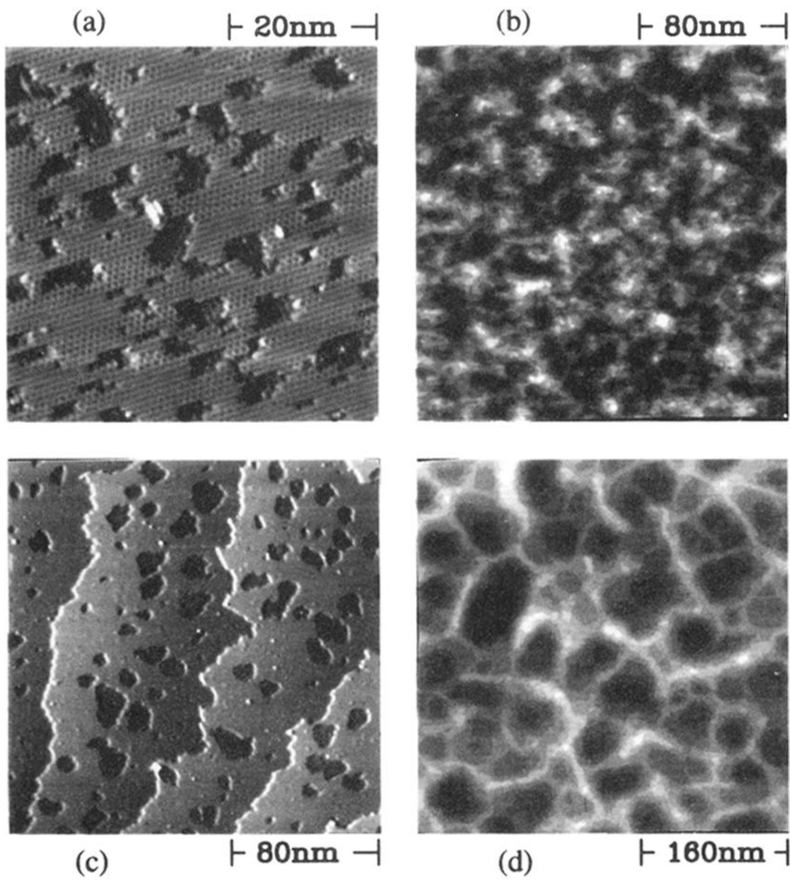

FIG. 4. STM images of Ge(001) etched by 240 Xe ions. Scale bars are shown next to each image. Number of monolayers removed and temperature during etching are: (a) 0.18, 220 °C; (b) 7.0, 220 °C; (c) 0.18, 295 °C; (d) 7.0, 295°C. In (a) and (c) the images have been high pass filtered to increase step edge contrast. In (b) and (d) no filter is used and the black-to-white gray scales are 0.9 nm and 1.3 nm, respectively.